HHS Public Access

Author manuscript

Adv Healthc Mater. Author manuscript; available in PMC 2019 May 01.

Published in final edited form as:

Adv Healthc Mater. 2018 May ; 7(9): e1701393. doi:10.1002/adhm.201701393.

Tough Composite Hydrogels with High Loading and Local Release of Biological Drugs

Dr. Jianyu Li,

John A. Paulson School of Engineering and Applied Sciences,Harvard University, Cambridge, MA 02138, USA

Wyss Institute for Biologically Inspired Engineering,Harvard University, Cambridge, MA 02138, USA

Dr. Eckhard Weber,

Novartis Institutes for BioMedical Research, Basel, Switzerland

Sabine Guth-Gundel,

Novartis Institutes for BioMedical Research, Basel, Switzerland

Michael Schuleit,

Novartis Institutes for BioMedical Research, Basel, Switzerland

Andreas Kuttler,

Novartis Institutes for BioMedical Research, Basel, Switzerland

Christine Halleux,

Novartis Institutes for BioMedical Research, Basel, Switzerland

Accart Nathalie,

Novartis Institutes for BioMedical Research, Basel, Switzerland

Arno Doelemeyer,

Novartis Institutes for BioMedical Research, Basel, Switzerland

Anne Basler,

Novartis Institutes for BioMedical Research, Basel, Switzerland

Bruno Tigani,

Novartis Institutes for BioMedical Research, Basel, Switzerland

Kuno Wuersch,

Novartis Institutes for BioMedical Research, Basel, Switzerland

Mara Fornaro,

Novartis Institutes for BioMedical Research, Basel, Switzerland

Dr. Michaela Kneissel,

Novartis Institutes for BioMedical Research, Basel, Switzerland

Alexander Stafford,

mooneyd@seas.harvard.edu.

John A. Paulson School of Engineering and Applied Sciences,Harvard University, Cambridge, MA 02138, USA

Wyss Institute for Biologically Inspired Engineering,Harvard University, Cambridge, MA 02138, USA

Dr. Benjamin R. Freedman, and
John A. Paulson School of Engineering and Applied Sciences,Harvard University, Cambridge, MA 02138, USA

Wyss Institute for Biologically Inspired Engineering,Harvard University, Cambridge, MA 02138, USA

Dr. David J. Mooney
John A. Paulson School of Engineering and Applied Sciences,Harvard University, Cambridge, MA 02138, USA

Wyss Institute for Biologically Inspired Engineering,Harvard University, Cambridge, MA 02138, USA

Abstract

Hydrogels are under active development for controlled drug delivery, but their clinical translation has been limited by low drug loading capacity, deficiencies in mechanical toughness and storage stability, and poor control over the drug release that often results in burst release and short release duration. This work reports a design of composite clay hydrogels, which simultaneously achieve a spectrum of mechanical, storage, and drug loading/releasing properties to address the critical needs from translational perspectives. The clay nanoparticles provide large surface areas to adsorb biological drugs, and assemble into microparticles that are physically trapped within and toughen hydrogel networks. The composite hydrogels demonstrate feasibility of storage, and extended release of large quantities of an insulin-like growth factor-1 mimetic protein (8 mg/mL) over four weeks. The release rate was primarily governed by ionic exchange and could be upregulated by low pH, which is typical for injured tissues. A rodent model of Achilles tendon injury was used to demonstrate that the composite hydrogels allow for highly extended and localized release of biological drugs in vivo, while demonstrating biodegradation and biocompatibility. These attributes make the composite hydrogel a promising system for drug delivery and regenerative medicine. [46,47,48]

Graphical Abstract

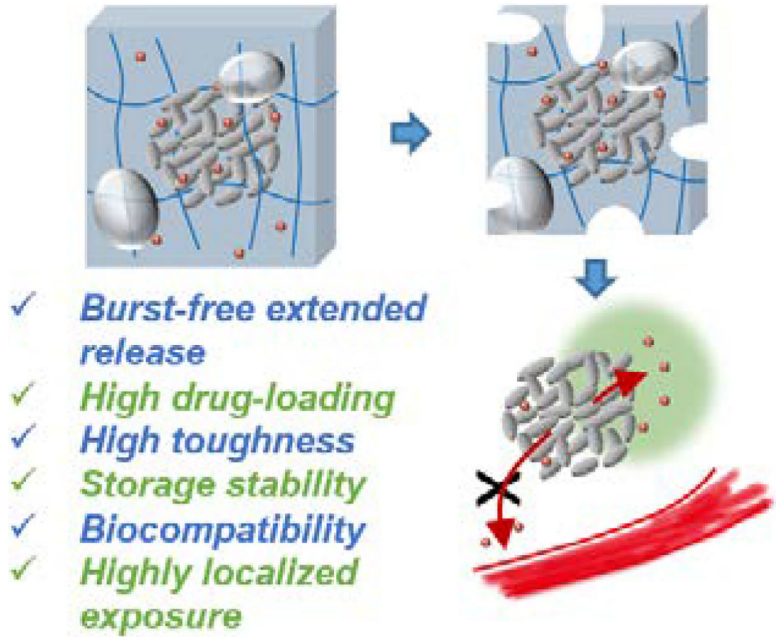

Keywords

Composite hydrogels; controlled delivery; biological drugs; regenerative medicine; tough hydrogels

1. Introduction

Effective drug administration often requires sophisticated control over the drug presentation to enhance therapeutic efficacy, avoid side effects, and increase patient compliance.[1] While increasing numbers of biological therapeutics are being developed and marketed,[2] their formulation and delivery poses substantial challenges due to their large size, susceptibility to denaturation and risks of side effects.[3,4] For controlled biological drug delivery, hydrogels are highly appealing owing to their mild hydrophilic matrix, which can minimize protein denaturation during incorporation and can protect labile proteins from harsh environments.[5,6]

The hydrophilic nature of hydrogels, however, often also results in low mechanical strength, storage instability and a trade-off between the drug loading capacity and their ability to provide sustained release. First, many hydrogels lose physical integrity during handling or functioning under dynamic tissue environments, which may change the drug-release property.[6,7] Second, the hydrated nature of these systems also makes their storage difficult, as the loss/gain of water may change the physical and drug-release properties of the hydrogels, and storage of the hydrogels in a hydrated state will lead to degradation if they are susceptible to hydrolysis.[8] More importantly, with increasing drug loading, the hydrogels typically lead to more significant burst release,[9] as the drug is often released freely via diffusion through the hydrated polymer network; as a consequence, the rapidly released drug may distribute into the blood circulation, resulting in undesired systemic

exposure.[10] For example, the burst release of bone morphogenetic proteins from collagen hydrogels led to undesirable side effects, including heterotopic ossification of soft tissue.[11] To achieve better control over release kinetics, one can either chemically modify the drugs and the hydrogels to allow for covalent linkage,[12] or encapsulate the drugs into nano- and micro-particles [like poly(lactide-co-glycolic acid), (PLGA)] that are then incorporated inside hydrogels.[13,14] Both approaches increase the complexity of the drug incorporation process, raise the risk of denaturation of biological drugs, and limit the drug loading capacity.

An ideal hydrogel delivery system, from a translational perspective, should combine high drug-loading capacity, mechanical toughness, storage stability, and allow for drug release over an extended time. Here we demonstrate a design of composite hydrogels that meets all these requirements. These composite hydrogels are composed of clay nanoparticles and a biodegradable alginate hydrogel network. The clay nanoparticles carrying negative charges on their surfaces can self-assemble into nano- and micro-sized particles depending on solvent conditions,[15] making the clay versatile drug carriers that can provide a large surface area to adsorb large quantities of charged drugs via electrostatic interactions, and allow for engineering their steric interactions with the hydrogel network.[16,17] The alginate network is formed by cross-linking alginate with calcium sulfate in a mild gelation condition, leading to highly biocompatible hydrogels;[18] their biodegradation is tunable (weeks to months) by using periodate oxidation to create hydrolytic acetal groups on the alginate chains.[8,19] Both the clay particles and alginate hydrogels have previously been used clinically (e.g., alginate gels are used as biological drug carriers in commercial products such as Emdogain[20] and Progenix,[21] and have undergone extensive animal testing.[17,18,22] Here we demonstrate high drug-loading capacity, high mechanical toughness of the composite hydrogels, and a capacity to release large quantities of a model biological drug with close clinic relevance, an insulin-like growth factor-1 (IGF1) mimetic protein conjugated with polyethylene glycol (PEG) over an extended period. The underlying release mechanism was elucidated, as well as its response to pH. In a rodent model of Achilles tendon injury, we demonstrated that the composite hydrogel delivery system led to sustained and localized release of the IGF1 mimetic protein, and was biodegradable while exhibiting good compatibility with the surrounding tissue.

2. Results

2.1. Design of Composite Hydrogels

Composite hydrogels were prepared with a facile approach combining clay inclusion, biodegradable hydrogels and lyophilization treatment. The resulting composite hydrogels consist of a structure in which clay nanoparticles assemble into micro-size particles embedded inside a degradable alginate network that has micro-sized cavities (**Figure 1**A). The multiscale characteristics include the individual clay nanoparticles on the nanometer scale, the 10’s of nanometer mesh size of the nanoporous alginate network, the assembly of clay nanoparticles on the micrometer scale, the cavities in the hydrogel of ~100 micrometers, and the bulk hydrogel on the millimeter scale. These together contribute to the mechanical, physical and drug-release properties of the composite hydrogels.

A synthetic clay (Laponite), which is comprised of nanodisks 25 nm diameter and 1 nm thickness, was used to bind the IGF1 mimetic protein (model protein drug). The microparticles that result from assembly of clay nanoparticles were distributed homogeneously inside the composite hydrogels. The average size of the clay microparticles was ~1.0 μm (Figure 1B), which was much larger than the size of the clay nanoparticles before assembly (Figure S1, Supporting Information). The size of the clay microparticles after assembly was consistent with other reports in the literature.[15,23] The clay microparticles provide binding sites for controlled release (Figure S2, Supporting Information). The size of microparticles is tunable by varying the solvent conditions such as pH, ionic strength, and macromolecular solutes.[15,23,24] Despite a degree of polydispersity, the minimum size of the particles was also much larger than the mesh size of the alginate network (typically tens of nanometers).[18] The size contrast enables the hydrogel matrix to entrap the clay particles via sufficiently large steric hindrance for slow drug release.[6]

The hydrogel matrix is composed of a mixture of non-oxidized and oxidized alginate, which is physically cross-linked with calcium ions (Figure 1C). The rate of degradation increases with the content of the oxidized alginate (Figure 1D). The slight increase of elastic modulus is likely due to further cross-linking following the initial gelation period. Both free drug and drug-loaded clay particles are expected to be released from the alginate hydrogel as it degrades, and the local environment (e.g., low pH in wound sites) may facilitate the drug release from the clay nanoparticles, together leading to a localized and extended release with minimal entry of the drug into the circulation.

2.2. Mechanical Properties

The lyophilization treatment was found to improve the mechanical properties of the composite hydrogels (**Figure 2**A and 2B). Lyophilization introduced cavities into the otherwise nanoporous alginate gels (Figure S3, Supporting Information); unlike interconnected pores in cryogels, the cavities of composite hydrogels were closed pores, which were expected not to change the overall diffusion properties of the matrix.[25] As closed cavities are known to soften and toughen solid matrices,[26] we hypothesize they may enhance the compliance and toughness of the composite hydrogels. Indeed, the composite hydrogels maintained low stiffness, despite the high clay content used for high protein loading; the hydrogel without lyophilization exhibited much higher stiffness than that of the composite hydrogels (Figure 2A). Previous studies have revealed that the inclusion of clay nanoparticles and no lyophilization stiffened hydrogels.[27,28] Moreover, the composite hydrogels with the cavities sustained 80% compressive strains without rupture, whereas the clay hydrogels without cavities failed below 50% compressive strains, similar to conventional alginate hydrogels (Figure 2B). A series of loading-unloading compression tests showed large hysteresis in the stress-strain curves, indicating that the composite hydrogels have effective energy-dissipating mechanisms (Figure S4, Supporting Information). The lyophilization led to high toughness and compliance of the composite hydrogels, which may benefit applications involving dynamic environments and mechanical loading.

2.3. Drug-loading Capacity

The effect of the clay on the protein drug and the hydrogel matrix was next investigated. PEGylation of proteins represents a principle to increase the stability and thus the half-life of biological drugs; various therapies with PEGylated proteins have been approved by regulatory authorities.[29] The clay nanoparticles were capable of binding a large amount of the PEGylated IGF1 mimetic protein (8.0 mg/mL for 8% clay), and the loading efficiency was found to depend on the clay concentration (Figure 2C). Typical biological drug loadings of hydrogels range from 0.01 to 1.0 mg/mL.[30–34] As the IGF1 mimetic protein carries a net positive charge at neutral pH (isoelectric point 9.36), it likely interacts with the negative surface of the clay nanoparticles via electrostatic attractions. Indeed, adsorption of the IGF1 mimetic protein led to an increase of zeta potential of the clay nanoparticles (Figure 2D). The protein loading capacity of the clay nanoparticles was found to be ~10%, which was higher than that of other types of particles (e.g., PLGA 0.1–1%) that have been similarly used to adsorb/encapsulate protein drugs.[13,14] This feature was attributed to the large surface area and high charge density of the clay nanoparticles, which was preserved after the assembly of clay particles. We also confirmed that the IGF1 mimetic protein released from the composite hydrogels remained bioactive, as assessed by its ability to induce phosphorylation of the IGF1 receptor on NIH-3T3 fibroblast cells (Figure S5, Supporting Information). The bioactivity of the drug released from the hydrogels was measured over time and compared to control protein drug placed directly in saline. The bioactivity of the drug in the release buffer increased with the release time, reaching a similar value as the control condition by 8 days, demonstrating release of bioactive drug over an extended period.

2.4. Burst-free Extended Release

We next investigated how the in vitro drug release properties of the composite hydrogels depend on incorporation of clay particles and lyophilization treatment. As the size of the individual protein molecules is typically smaller than that of the meshes of the hydrogel matrix, we hypothesize that the inclusion of clay nanoparticles is critical for effective control over the protein release. **Figure 3**A and 3B illustrated the effect of clay nanoparticles on the early release, focusing on the initial burst release. Indeed, increasing the clay content reduced the protein release rate (Figure 3A). Gels containing 6% and 8% clay led to a nearly zero-order release, with little initial burst. In contrast, the alginate gels without clay showed a significant burst release (>60%), and the duration of release was less than 3 days (Figure 3B). We also converted the alginate to sulfated alginate to promote stronger electrostatic interactions with the protein via the sulfate groups,[35] which, however, still led to significant burst release of the protein as compared to the composite hydrogels (Figure S6, Supporting Information). We further determined that lyophilization led to a slight increase in the burst release of the protein, as compared to the unlyophilized gels, but the subsequent release kinetics were similar (Figure S7, Supporting Information); after being storage for 15 days and then rehydrated, the composite hydrogels also showed similar release characteristics as compared to the as-prepared gels (Figure S8, Supporting Information). This was attributed to the fact that lyophilization removes the water without changing the overall diffusion properties of the matrix, so that the degradable polymer matrix remained dry and stable

throughout storage. The results show that the lyophilization treatment can prevent degradation of the composite hydrogels before implementation, and greatly improve the ease and stability of the composite hydrogels for storage.

2.5. pH-triggered Extended Release

As the electrostatic nature of the protein-clay interactions implied that the release may respond to environmental conditions like pH,[15] we next examined the dependence of the release profile on pH. As low pH will protonate the negative charges on the clay nanoparticles, we hypothesized that it would weaken the protein-clay attraction and increase the protein release rate. The pH of the release medium was varied from 5.0 to 7.4, as this range of pH is typically found at wound sites.[36] Interestingly, the release was more rapid and complete at the investigated lower pH as compared to neutral pH (Figure 3C). The release triggered by the pH remained in a slow and extended manner, in contrast to other pH-triggered systems that exhibited burst drug release after triggering. The effect of pH was sufficient in upregulating the drug release, although the range of pH was much higher than the pKa of carboxylate groups that were believed to interact with the model drug. The results showed that the release profile at pH 6 was more linear compared to those at other pH, and that the drug release behavior was highly sensitive to the pH in a physiologically relevant range. The impact of low pH on the potential for drug-clay association was also validated with zeta-potential measurements, in which the negative charge density of clay particles was significantly reduced with decreasing pH (Figure 3D). These results support the role of ionic exchange in governing drug release from this system, and suggest the drug release would preferentially occur at wound sites, as contrasted to undamaged tissues.

2.6. Release Mechanism of Ionic Exchange

The underlying mechanism governing protein incorporation and release from the composite hydrogels was next examined. The IGF1 mimetic protein might be physically encapsulated within the composite hydrogels, or electrostatically adsorbed onto the clay particles. Given the pH-responsive release profiles, we postulate that the electrostatic interaction between the clay nanoparticles and the drug dominates the drug release. To examine this hypothesis, we determined the ratio of incorporated proteins adsorbed onto the clay nanoparticles to those not adsorbed onto the clay nanoparticles. The calcium cross-linked alginate hydrogel was digested immediately after fabrication with a combination of alginate lyase and EDTA to chelate calcium, and the recovery of free protein was assessed. Only, a small portion of protein (around 15% of the nominal load) was recovered, indicating most of the protein was adsorbed onto the clay nanoparticles (Figure S9, Supporting Information). Under the context of composite hydrogels, the drug loading varied with the clay content, and the drug loading efficiency was similar to that shown in Figure 2C (Figure S9, Supporting Information). The alginate hydrogels likely contribute to additional electrostatic and steric effects on drug encapsulation; however, compared to the effect of clay nanoparticles, this contribution is small. This result was consistent with the minimal burst release noted in the in vitro release studies, and further confirmed a dominant effect of the clay on the overall drug encapsulation. To confirm that the remainder protein was adsorbed onto the clay nanoparticles, we developed an ionic exchange technique to force drug disassociation from clay. We hypothesized that a strong positively charged polymer (polyallylamine) would

compete for the negatively charged binding sites on the clay to dissociate the protein from the clay nanoparticles. Indeed, treatment of clay, obtained from digested composite hydrogels, with polyallylamine led to a recovery of the remainder of hydrogel-incorporated drug, and closed the mass balance for the loaded protein (Figure S9, Supporting Information). These studies reveal how the protein is partitioned inside the composite hydrogels, and suggest that ionic exchange is the dominant mechanism of slow protein release from the composite hydrogels.

2.7. Biodegradation and Biocompatibility

We next evaluated the composite hydrogels in a rodent Achilles tendon injury model in vivo, to mimic one potential application of this system. This approach may be particularly important for the treatment of tendon injury,[37] whereas previous studies delivering IGF-1 have utilized direct injection[38] or gene therapy,[39] which are not able to provide local controlled release and have short half-lives. Scaffolds of the composite hydrogels were surgically implanted on top of the site of Achilles tendon injury (**Figure 4**A). After 1 and 2 weeks, the implant and the surrounding tissues were evaluated for in vivo biodegradation and tissue compatibility. The histological assessment revealed that the implanted composite hydrogels degraded into multiple smaller fragments within one week, and over time the fragments were increasingly separated by small strands of fibroblasts (Figure 4B). The complete degradation of the composite hydrogels is estimated to occur around five weeks, as based on in vivo degradation analysis (Figure S10, Supporting Information). The degradation profiles were consistent with previous studies for similar hydrogels.[8,32,33] The composite hydrogels integrated well into the surrounding granulation tissue. Inflammatory cell infiltrates were absent or minimal, consisting of mononuclear cells, macrophages and only few foreign-body granulomas. Popliteal lymph nodes were relatively inactive with absent or small germinal centers. Altogether, the composite hydrogels did not induce excessive inflammation or adverse tissue reactions in the Achilles tendon injury model and the healing of the tendon injury was structurally similar to controls with no implantation of hydrogels. Based on these results, we conclude that the composite hydrogels are biodegradable and tissue compatible in vivo.

2.8. Extremely Localized Drug Presentation In Vivo

In the same rodent Achilles tendon injury model, in vivo release of the IGF1 mimetic protein was assessed. The composite hydrogels containing 6% clay were tested. They increased and prolonged exposure of the IGF1 mimetic protein to the tendon, as compared to the simple bolus injection of the same quantity of protein (Figure 4C). The levels of the IGF1 mimetic protein detected in serum showed an opposite trend: the protein administrated by bolus injection penetrated into the blood circulation, in contrast to negligible detected serum levels with the composite hydrogels (Figure 4D). The composite hydrogels led to a significant contrast in the ratio of the protein exposure to Achilles tendon versus serum, which is four orders of magnitude higher than that resulting from bolus injection (Figure 4E). To explicitly reveal confined IGF1 mimetic protein distribution in the injured Achilles tendon in vivo, the protein was conjugated with VivoTag® 680, and delivered with the composite hydrogels. Examination of histological sections over 8 days after scaffold implantation revealed confined protein distribution in the tendon (Figure 4F). The confined area of protein

distribution in the Achilles tendon decreased from day 1 to day 8 post-implantation. The scattering of fluorescence signal intensity remained similar over time (Figure 4G). These results demonstrated that the design of composite hydrogels led to extremely extended and highly localized release of the IGF1 mimetic protein, which may offer a novel approach to reduce systemic side effects of growth factors.[10]

3. Discussion

Compared to other hydrogel delivery systems, the composite hydrogels achieved high drug loading and extended release simultaneously. **Figure 5** summarized the drug loading capacity and extended releasing properties of various hydrogel delivery systems, in which the extended releasing property is quantified with the time when the system releases out half of the loaded drug (half-life time). The comparison shown here was based on values extracted from the literature; a head-to-head comparison was not performed due to potential variations in experimental setups and testing strategies in different labs.

Many systems suffer limited drug loading capacities (0.01–1 mg/mL) and relatively short release durations (<5 days). For instance, despite many advantages of PLGA-based systems for controlled delivery, many studies have indicated that a major hurdle limiting their clinical use is the relatively low drug loading efficiency.[40–42] A recent advance highlights a potential remedy with encapsulation-free PLGA nanoparticles.[14] They utilized the negative-charged surfaces of the nanoparticles to absorb protein therapeutics, leading to burst-free and extended protein release. Although this approach is promising, the drug loading capacity was below 1 mg/mL, possibly due to relatively small surface area and low charge density of the PLGA nanoparticles.[14] Another progress is the development of degradable PEG hydrogels slow down the protein release. This mechanism was not applicable to small molecule drugs, and limited by coupling between the stiffness and the drug releasing properties.[31] In comparison, the composite hydrogels achieved simultaneously high mechanical toughness, and superior drug loading and sustained releasing capacities.

The incorporation of clay nanoparticles is a facile and versatile strategy for controlled protein delivery. Previous studies have demonstrated that the clay can interact with a variety of proteins, including vascular endothelial growth factor-165, bone morphogenic protein 2, recombinant murine granulocyte-macrophage colony-stimulating factor, and interleukin 15.[17,22,43] This work reports the first demonstration of the approach for delivery of PEGylated therapeutics, which are increasingly being used in the clinic. The non-specific electrostatic interactions enabled by clay nanoparticles will also likely allow co-delivery of multiple proteins, which is of increasing importance in regenerative medicine.[44,45]

Our preliminary results indicated that the tested formulation of the composite hydrogels led to limited tendon regeneration. The limitations of the current formulation could include suboptimal drug presentation in vivo (pulsatile release may be preferable as versus sustained), a greater required threshold of drug exposure, even higher drug loading and release duration. Further studies are needed to identify and optimize the limiting factors for this specific model of Achilles tendon regeneration.

4. Conclusion

Controlled delivery using hydrogels could leverage therapeutic outcomes of biological drugs, but are facing hurdles for clinic translation, including mechanical weakness, storage instability, burst release, short release duration, and undesirable systemic exposure of the drugs. This work presents a design of composite hydrogels to address the critical needs of local drug release from practical perspectives. Such hydrogels tolerate large deformation, and achieve simultaneously high drug loading, extended release over weeks, and extremely localized drug presentation without significant systemic exposure in vivo. They also exhibit shelf-life stability for easy storage, supportive tissue compatibility, and biodegradability without overt tissue response over time. The unique combination of mechanical, physical and drug delivery properties might aid the clinic translation of hydrogel drug delivery systems.

5. Experimental Section

Materials.

Ultrapure sodium alginate with low endotoxin levels (MVG and VLVG; ProNova Biomedical AS) was used. MVG and VLVG denote medium viscosity and very low viscosity alginate, both with minimum 60% guluronate monomer units. The oxidized alginate, with an oxidation degree of 1%, was prepared by sodium periodate oxidation, according to a protocol reported previously.[8] The resulting aldehydes were selectively reduced to alcohols using sodium borohydride (Pfaltz & Bauer). A model PEGylated biological drug, an insulin-like growth factor-1 (IGF1) mimetic protein conjugated with a linear polyethylene glycol (PEG) chain, with a final molecular weight of 41219 Da and isoelectric point of 9.36 (Novartis Pharma AG), was used. A synthetic clay (Laponite; BYK Additives & Instruments) was also used.

VT680 Fluorescence Labeling of the IGF1 Mimetic Protein.

The fluorescent dye VivoTag® 680 XL (PerkinElmer) is an amine reactive fluorochrome (maximum absorbance 668 nm; excitation maximum 665 nm; peak emission 688 nm). The dye was reconstituted with DMSO at a concentration of 10 mg/mL and this stock solution was stored at −20°C. IGF1 mimetic protein (1–5 mg/mL) in 10 mM PBS pH7.4 was mixed with 1 M $NaHCO_3$ to adjust pH to 9. Then 4-molar equivalent of VivoTag® 680 XL in DMSO was added and the solution was incubated at 8°C for 4 hours. Free dye was removed by purification on ÄKTA Purifier (GE Healthcare, HiPrep Desalting column, PBS). The first fraction corresponding to the VivoTag® 680 XL labeled IGF1 mimetic protein was collected and concentrated using Amicon centrifugal filter (MWCO, 10 kDa). The product was characterized by size exclusion chromatography, UV/Vis spectroscopy, and BCA assay to determine protein and dye concentrations, and degree of labeling of the conjugate.

Hydrogel Synthesis.

The composite hydrogels were prepared in a facile three-step protocol. (1) Drug loading: an alginate solution was prepared by dissolving the ultra-pure alginate and the oxidized alginate in HBSS without calcium and magnesium, in which the ratio of MVG and VLVG was fixed

at 25:75. The fraction of the oxidized alginate in the alginate was fixed at 25%, unless stated otherwise. A certain amount of clay was dissolved and dispersed in HBSS under vigorous vortexing to form clay nanoparticles. The mixture was syringe-mixed with the alginate solution, the un-labelled or VT680-labelled IGF1 mimetic protein subsequently, and then incubated for 30 minutes to allow for the clay-protein adsorption. The final concentrations of clay nanoparticles were varied from 4% to 8% in the composite hydrogels. (2) Calcium crosslinking: the solution of alginate, clay and protein was syringe-mixed with calcium sulfate slurries to form a hydrogel, which was stored overnight to ensure the ionic crosslinking was complete. The final concentrations of alginate and calcium sulfate were fixed at 3.6% and 38 mM. The final concentration of the un-labelled or VT680-labelled IGF1 mimetic protein was fixed at 8 mg/mL (corresponds to 200 μg per scaffold of the hydrogel composite), unless stated otherwise. (3) Lyophilization: the hydrogel of 5×8×0.65 mm^3 was frozen at −80°C for 6 hours, and then lyophilized with a freeze-dryer (SP Scientific Freezemobile) for 2–3 days. After lyophilization, the dry scaffold of the composite hydrogel was stored at +4°C before usage.

Confocal Imaging.

Confocal microscopy (Carl Zeiss Upright LSM 710 Microscope) was used to image the clay nanoparticles and microparticles embedded inside the composite hydrogels containing Rhodamine-B labelled alginate (Alg-RB). The composite hydrogels were prepared as described above, except 5% of alginate was rhodamine-B labeled. The images were recorded with a water immersion lens of 40× magnification and the excitation wavelength at 556 nm. The clay attracted the Alg-RB leading to high-intensity signal areas around particles owing to their positively charged rims.

In vitro Release Study.

The release profiles of IGF1 mimetic protein were characterized with high performance liquid chromatography (HPLC). The HPLC analysis was performed on Agilent 1200 series HPLC system, equipped with a column (YMC-Pack ODS-AQ 150mm × 4.6mml, 3μm; AQ20S03–1546WT) for analytical reversed phase chromatography. Each hydrogel (5×8×0.65 mm^3) was first hydrated with 20 μL distilled water for at least 30 minutes, and then soaked in 0.5 mL of the release medium PBS containing divalent ions (cPBS) at 37°C. The release medium was changed routinely (up to 30 days) and collected; aliquots of 100 μL were used for the HPLC analysis. The two mobile phases were 10% acetonitrile (ACN) plus 0.1% (v/v) trifluoroacetic acid (TFA) and 80% ACN plus 0.1% TFA, respectively. The injection volume was 100 μL and the flow rate kept at 1 mL/min (See Table. S1 for details). The temperature of the autosampler and the column was set at +4°C and +65°C, respectively. The IGF1 mimetic protein was detected with variable wavelength detector at 215 nm and corresponded to a peak at a retention time of 12 minutes (Figure S11, Supporting Information). The standard curve of the protein dissolved in cPBS was determined by varying the IGF1 mimetic protein concentration from 5 to 200 μg/mL in a series of calibration solutions, which were used to calculate the protein concentration in the release medium (Figure S11, Supporting Information).

Statistics.

Statistical analysis in this study was performed using embedded algorithms in a commercial software GraphPad Prism 6. One-way Analysis of Variance (ANOVA) tests were used to analyze multiple sets of data, while student's t tests were used in the analysis of experiment involving two sets of data. The sample sizes (N), means and standard deviations (mean ± SD) for each experiment are shown in the manuscript. The *P* values were calculated by ANOVA or student's t tests. The levels of significance are labeled with **P*≤0.05; ***P*≤0.01; ****P*≤0.001; *****P*≤0.0001.

Drug Loading Study.

The content of clay nanoparticles dissolved into cPBS was varied between 0.3 to 8 wt%, while the protein concentration was fixed at 8 mg/mL. The clay-protein mixture was incubated with vortexing for 30 minutes, and centrifuged at 2000 rcf for 5 minutes. The supernatants were collected and analyzed by the HPLC technique to quantify the remaining protein concentration in the supernatant (C_{free}). The concentration of the IGF1 mimetic protein adsorbed onto the clay nanoparticles was then calculated by subtracting C_{free} from 8 mg/mL.

Forced Dissociation Study.

The composite hydrogels loaded with the IGF1 mimetic protein were fully digested with 100 mM EDTA solution and alginate lyase (2 units/mL) sequentially. After centrifugation (2000 rcf for 5 minutes), the first supernatant was collected for the HPLC analysis; the protein detected at this step was not tightly adsorbed onto the clay nanoparticles. The sediment of the clay nanoparticles was treated with 2% polyallylamine aqueous solution (PAA; 750,000 Da; Sigma) repeatedly (up to 3 times). The supernatants after each PAA treatment were collected for the HPLC analysis. The sum of the protein recovered from the PAA treatment was the total amount of the protein tightly adsorbed onto the clay nanoparticles. The protein concentration was calculated based on a standard curve of the IGF1 mimetic protein dissolved in PAA solutions in the concentration range from 5 to 800 μg/mL (Figure S11, Supporting Information).

Zeta Potential Measurements.

The clay nanoparticles were suspended in cPBS at 6%, with/without the model protein of 8 mg/mL. The suspension was vortexed vigorously for 30 minutes, and then diluted with cPBS of varying pH from 5.0, 6.0 to 7.4. The resulting suspension was analyzed with a particle size analyzer (Malvern zen3600) for zeta potentials.

Mechanical Tests.

Compression tests were performed with an Instron machine (Instron 3342 single column apparatus with a 1000N load cell). The strain rate was fixed at 200% per minute. Both the force and extension were recorded. The elastic modulus was defined as the tangent of the stress-strain curve at the range of small strains (1–10%). In the biodegradation tests, the composite hydrogels containing different fractions of oxidized alginate were hydrated, sealed and stored at +4^{o}C for 2 weeks, followed by compression testing. For the loading-

unloading tests, the composite hydrogels of varying clay contents were subject to three levels of maximum compressive strains (10%, 50% and 80%).

In Vitro Bioactivity Assessment.

The bioactivity of the IGF1 mimetic protein was assessed based on phosphorylation of the type I Insulin-like growth factor receptor (IGF1R) on NIH-3T3 cells, as detected by ELISA. The composite hydrogels were fabricated in Boston, MA, USA, and then shipped to Basel, Switzerland for the bioactivity tests. The duration of shipping and storage was 3–5 days. NIH3T3 cells overexpressing human InsR (NIH3T3-InsR) were seeded at 6000 cells/well (96-well plate format) in DMEM high glucose containing 10% FBS, 1% sodium pyruvate, 2mM L-glutamine, 10mM HEPES, 100U/ml penicillin and 100 μg/ml streptomycin (all medium components from Life Technologies) and incubated overnight at 37°C in a humidified incubator with 5% CO_2. Thereafter, cells were serum-starved, in DMEM high glucose, 0.1% BSA, 1% sodium pyruvate, 2mM L-glutamine, 10mM HEPES, 100U/ml penicillin and 100ug/ml streptomycin for 1.5h at 37°C, 5% CO_2 before being stimulated either with the IGF1 mimetic protein released from the composite hydrogel or with freshly dissolved IGF1 mimetic protein for 1h at 37°C, 5% CO_2. Finally, cells were lysed in 1× TBS, 1× TritonX-100, 0.005M EDTA, 1× protease phosphatase inhibitor (Thermo Scientific) for 30–45 minutes on a horizontal shaker at +4°C. IGF-1R phosphorylation was analyzed by ELISA using the same procedure as the DuoSet IC human phosphor-IGF-1R (R&D systems) with the following modifications: the capture antibody (R&D MAB391) was diluted to 4 ug/ml in PBS, wells were washed with 300ul/well of PBS-Tween (Millipore, 524653), wells were blocked with 200ul/well 1% BSA in PBS, phosphorylation was detected using an antibody HRP-anti-phosphotyrosine (R&D, HAM1676) and the luminescent signal was detected with a chemiluminescence substrate (Pierce, 37069).

Rat Achilles Tendon Injury Model.

Adult female Sprague Dawley rats (age: 9 months; body weight: 300 to 400 g; supplier: Janvier) were housed according to standard conditions with food and water ad libitum and light/dark cycle of 12/12 hours. The animal experimental protocols were carried out according to guidelines and were approved by the Ethics Committee of Canton of Basel-City, Switzerland. Surgical procedures were performed under general inhalation anesthesia with isoflurane (1.5 to 3 vol%). Rats were prepared for aseptic surgery and were placed on a surgery table with the right foot fixed in a 90° downward-facing position relative to the tibia using a custom-tailored holder. A 10-mm skin incision was performed dorsal proximal to the calcaneus bone and the exposed Achilles tendon complex including the plantaris tendon was transected transversally at the mid-portion level. The Achilles tenotomy was immediately repaired by end-to-end anastomosis applying a three-loop pulley suture (Prolene 5–0, Ethicon). Subsequently, a disc-like scaffold of the composite hydrogel loaded with un-labelled or VT680-labelled IGF1 mimetic protein (diameter: 5 mm; height: 0.6 mm) was placed on top of the Achilles tendon anastomosis and the skin was then closed by a continuous intra-cutaneous suture (Safil 6–0, Braun). Animals were sacrificed at defined time points post-implantation with CO_2 to excise tissue and blood for the time course assessment of release of IGF1 mimetic release and the tissue compatibility of the composite hydrogel.

In Vivo Release Assessment.

The concentration of the IGF1 mimetic protein was measured in serum and Achilles tendon tissue. Snap-frozen Achilles tendon samples were homogenized using Freezer/Mill® technology (SPEX SamplePrep) for cryogenic grinding and pulverizing. The samples were transferred into a sealed microvial and 50 μL of a HALT protease and phosphatase inhibitor (Thermo Scientific #78442) was added in 1% v/v in Pierce Lysis RIPA buffer (Thermo Scientific #89901). Grinding of the samples was performed 2 times for 2 minutes with a steel impactor frequency of 12 cycles per second. The homogenized Achilles tendon samples were lysed in 500 μL of Pierce Lysis RIPA buffer containing 1% (v/v) HALT protease and phosphatase inhibitor for 1.5 hours on ice and vortexed every 15 minutes. At the end, the lysed samples were centrifuged for 15 minutes at 14,000 r.p.m. at +4°C. Bioanalysis of the IGF1 mimetic protein in serum and the Achilles tendon lysates was performed using a sandwich ELISA (Novartis Pharma AG), which is selective for the used IGF1 mimetic protein and does not cross-react with the endogenous IGF1 protein. Microtiter plate wells (Costar) were coated with 100 μL mouse monoclonal antibody specific for the recombinant protein (10 μg/mL), diluted in carbonate-bicarbonate buffer (Thermo Scientific) and incubated overnight at +4°C. The wells were washed three times with 300 μL of 1 × KPL wash buffer (Kirkegaard & Perry) and subsequently blocked with 300 μL of 1 × KPL milk diluent (Kirkegaard & Perry) for 1 hour at room temperature. After washing four times with 300 μL of 1 × KPL wash buffer, 100 μL of Achilles tendon lysate diluted in Pierce Lysis RIPA buffer or 100 μL of serum samples appropriately diluted in control serum were added. The reference standard was diluted to yield concentrations of calibration samples ranging from 0.3 ng/mL to 160 ng/mL and 100 μL of each concentration were added to appropriate wells of the plate together with Pierce Lysis RIPA buffer or control serum as negative control. The plates were incubated for 2 hours at room temperature, washed three times with 1 × KPL wash buffer followed by another incubation of 90 minutes with 100 μL per well each of biotinylated anti-hIGF-1 antibody (80 ng/mL, R&D). After washing four times with 300 μl of 1 × KPL wash buffer, the wells were subsequently incubated with 100 μL of streptavidin-horseradish-peroxidase (R&D) for 20 minutes at room temperature. After washing three times as described above the plates were incubated with 100 μL substrate reagents (R&D #DY999) for 20 minutes at room temperature. The color reaction was stopped by adding 50 μL of stop solution (2 N sulfuric acid) to each well, and absorbance was read at 450 nm on a Synergy 2 ELISA reader (BioTek). The data were analyzed using a 4-parameter curve fitting program of GEN5 (BioTek).

In Vivo Tissue Compatibility Assessment.

Histopathology and fluorescence microscopy of the implanted composite hydrogel scaffold loaded with the un-labelled or VT680-labelled IGF1 mimetic protein was performed on sections of the lower hind limbs. Limbs were collected and immersed in 10% neutral buffered formalin for 72 hours and then decalcified in Immunocal™ (Decal Chemical Corp) for 5–7 days with daily changes. After bisection in the median anatomic plane to expose the mid-plane of the Achilles tendon, samples were dehydrated and paraffin embedded and then cut in 5-μm thick sagittal sections for staining with hematoxylin (3 minutes) and eosin (30 seconds) using a ST5010 Autostainer XL (Leica). In order to observe the fluorescence signal associated to VT680 labeling of IGF1 mimetic protein, 5-μm thick sagittal sections were

deparaffinized, rehydrated, and stained with 0.5μg/mL of 4', 6-DiAmidine, 2'-PhenylIndole (DAPI, Roche) and mounted in Mowiol™ (Calbiochem) aqueous mounting medium. HE- and DAPI-stained slides were scanned with an Aperio slide scanner (Leica) or a VS-120 slide scanner (Olympus) equipped with filter cubes dedicated for DAPI (excitation 350±50 nm, emission 457±30 nm) and for VT680 (Cy5, excitation 635±20 nm - emission 685±40 nm) observations.

The quantification of the fluorescence signal associated with the VT680-labelled IGF1 mimetic protein was performed on whole slide scans using HALO image analysis software (Indica Labs). The HE- and DAPI-stained slide scans were co-registered using the image registration feature of HALO. The HE-stained slide scans guided the definition of the region of interest, i.e., the total Achilles tendon area from the calcaneus bone insertion to the gastrocnemius muscle junction. The area annotations from the HE-stained slide scans were automatically transferred to the co-registered DAPI-stained slide scans. The fluorescence signal was quantified as areas of weak, moderate and strong fluorescence positive signals in the region of interest using the 'Area Quantification FL v1.0' algorithm. The qualitative histopathology assessment of tissue compatibility was performed on HE-stained slides by two independent pathologists.

Supplementary Material

Refer to Web version on PubMed Central for supplementary material.

Acknowledgements

This work was supported by award A21448 from Novartis Pharmaceuticals Corporation, the National Institute of Dental & Craniofacial Research of the National Institutes of Health (R01DE0130333), and support from the NSF MRSEC at Harvard University (DMR-1420570). J.L., E.W., S.G., M.S., A.S., and D.J.M. designed the experiments. J.L., E.W., S.G., M.S., A.K., C.H., N.A., A.D., A.B., B.T., K.W., M.F., M.K., A.S., and B.R.F. performed the experiments. All authors analyzed the data and wrote the paper. The authors state no competing interests.

References

[1]. Langer R, Nature 1998, 392, 5. [PubMed: 9579855]

[2]. BBC, Global markets for bioengineered protein drugs. BBC Res. 2014.

[3]. Mitragotri S, Burke PA, Langer R, Nat. Rev. Drug Discov 2014, 13, 655. [PubMed: 25103255]

[4]. Pakulska MM, Miersch S, Shoichet MS, Science 2016, 351, aac4750. [PubMed: 26989257]

[5]. Censi R, Di P, Vermonden T, Hennink WE, Chem. Rev 2012, 161, 680.

[6]. Li J, Mooney DJ, Nat. Rev. Mater 2016, 1, 16071. [PubMed: 29657852]

[7]. Li L, Yan B, Yang J, Chen L, Zeng H, Adv. Mater 2015, 27, 1294. [PubMed: 25581601]

[8]. Boontheekul T, Kong HJ, Mooney DJ, Biomaterials 2005, 26, 2455. [PubMed: 15585248]

[9]. Huang X, Brazel CS, J. Control. Release 2001, 73, 121. [PubMed: 11516493]

[10]. Martino MM, Briquez PS, Güç E, Tortelli F, Kilarski WW, Metzger S, Rice JJ, Kuhn GA, Müller R, Swartz MA, Hubbell JA, Science 2014, 343, 885. [PubMed: 24558160]

[11]. Shields LBE, Raque GH, Glassman SD, Campbell M, Vitaz T, Harpring J, Shields CB, Spine 2006, 31, 542. [PubMed: 16508549]

[12]. Ashley GW, Henise J, Reid R, V Santi D, Proc. Natl. Acad. Sci. U. S. A 2013, 110, 2318. [PubMed: 23345437]

[13]. Geng H, Song H, Qi J, Cui D, Nanoscale Res. Lett 2011, 6, 312. [PubMed: 21711840]

[14]. Pakulska MM, Elliott Donaghue I, Obermeyer JM, Tuladhar A, McLaughlin CK, Shendruk TN, Shoichet MS, Sci. Adv 2016, 2, e1600519. [PubMed: 27386554]

[15]. Wang S, Wu Y, Guo R, Huang Y, Wen S, Shen M, Wang J, Shi X, Langmuir 2013, 29, 5030. [PubMed: 23419072]

[16]. Dawson JI, Kanczler JM, Yang XB, Attard GS, Oreffo ROC, Adv. Mater 2011, 23, 3304. [PubMed: 21661063]

[17]. Dawson JI, Oreffo ROC, Adv. Mater 2013, 25, 4069. [PubMed: 23722321]

[18]. Lee KY, Mooney DJ, Prog. Polym. Sci 2012, 37, 106. [PubMed: 22125349]

[19]. Kong HJ, Kaigler D, Kim K, Mooney DJ, Biomacromolecules 2004, 5, 1720. [PubMed: 15360280]

[20]. Heijl L, Heden G, Svärdström G, Ostgren A, J. Clin. Periodontol 1997, 24, 705. [PubMed: 9310876]

[21]. Smucker JD, Fredericks DC, Iowa Orthop. J 2012, 32, 54. [PubMed: 23576922]

[22]. Gibbs DMR, Black CRM, Hulsart-Billstrom G, Shi P, Scarpa E, Oreffo ROC, Dawson JI, Biomaterials 2016, 99, 16. [PubMed: 27209259]

[23]. Takahashi T, Yamada Y, Kataoka K, Nagasaki Y, J. Control. Release 2005, 107, 408. [PubMed: 16171884]

[24]. Huang AY, Berg JC, J. Colloid Interface Sci 2006, 296, 159. [PubMed: 16182304]

[25]. A Bencherif S, Sands RW, Bhatta D, Arany P, Verbeke CS, A Edwards D, Mooney DJ, Proc. Natl. Acad. Sci. U. S. A 2012, 109, 19590. [PubMed: 23150549]

[26]. Gibson L, Ashby M, Cellular solids; Cambridge University Press, 1997.

[27]. Wang J, Lin L, Cheng Q, Jiang L, Angew. Chemie - Int. Ed 2012, 51, 4676.

[28]. Chang C-W, van Spreeuwel A, Zhang C, Varghese S, Soft Matter 2010, 6, 5157.

[29]. Greenwald RB, Choe YH, Mcguire J, Conover CD, Adv. Drug Deliv. Rev 2003, 55, 217. [PubMed: 12564978]

[30]. Ishii S, Kaneko J, Nagasaki Y, Biomaterials 2016, 84, 210. [PubMed: 26828685]

[31]. O'Shea TM, Aimetti AA, Kim E, Yesilyurt V, Langer R, Adv. Mater 2015, 27, 65. [PubMed: 25381960]

[32]. Silva EA, Mooney DJ, Biomaterials 2010, 31, 1235. [PubMed: 19906422]

[33]. Silva EA, Mooney DJ, J. Thromb. Haemost 2007, 5, 590. [PubMed: 17229044]

[34]. Bencherif SA, Warren Sands R, Ali OA, Li WA, Lewin SA, Braschler TM, Shih T-Y, Verbeke CS, Bhatta D, Dranoff G, Mooney DJ, Nat. Commun 2015, 6, 7556. [PubMed: 26265369]

[35]. Fan L, Jiang L, Xu Y, Zhou Y, Shen Y, Xie W, Long Z, Zhou J, Carbohydr. Polym 2011, 83, 1797.

[36]. Gethin G, Wounds UK. 2007, 3, 52.

[37]. Caliari SR, Harley BAC, Tissue Eng. Part A 2013, 19, 1100. [PubMed: 23157454]

[38]. Hansen M, Boesen A, Holm L, Flyvbjerg A, Langberg H, Kjaer M, Scand. J. Med. Sci. Sport 2013, 23, 614.

[39]. Tang Y, Leng Q, Xiang X, Zhang L, Yang Y, Qiu L, Gene Ther. 2015, 22, 610. [PubMed: 25840275]

[40]. Peracchia MT, Gref R, Minamitake Y, Domb A, Lotan N, Langer R, J. Control. Release 1997, 46, 223.

[41]. Govender T, Stolnik S, Garnett MC, Illum L, Davis SS, J. Control. Release 1999, 57, 171. [PubMed: 9971898]

[42]. Danhier F, Ansorena E, Silva JM, Coco R, Le Breton A, Préat V, J. Control. Release 2012, 161, 505. [PubMed: 22353619]

[43]. Koshy ST, Zhang DKY, Grolman JM, Stafford AG, Mooney DJ, Acta Biomater. 2017, 65, 36. [PubMed: 29128539]

[44]. Richardson TP, Peters MC, Ennett a B., Mooney DJ, Nat. Biotechnol. 2001, 19, 1029. [PubMed: 11689847]

[45]. Wylie RG, Ahsan S, Aizawa Y, Maxwell KL, Morshead CM, Shoichet MS, Nat. Mater 2011, 10, 799. [PubMed: 21874004]

[46]. Vulic K, Shoichet MS, J. Am. Chem. Soc 2012, 134, 882. [PubMed: 22201513]

[47]. Tellechea A, Silva EA, Min J, Leal EC, Auster ME, Pradhan-Nabzdyk L, Shih W, Mooney DJ, Veves A, Int. J. Low. Extrem. Wounds 2015, 14, 146. [PubMed: 26032947]

[48]. Kolambkar YM, Dupont KM, Boerckel JD, Huebsch N, Mooney DJ, Hutmacher DW, Guldberg RE, Biomaterials 2011, 32, 65. [PubMed: 20864165]

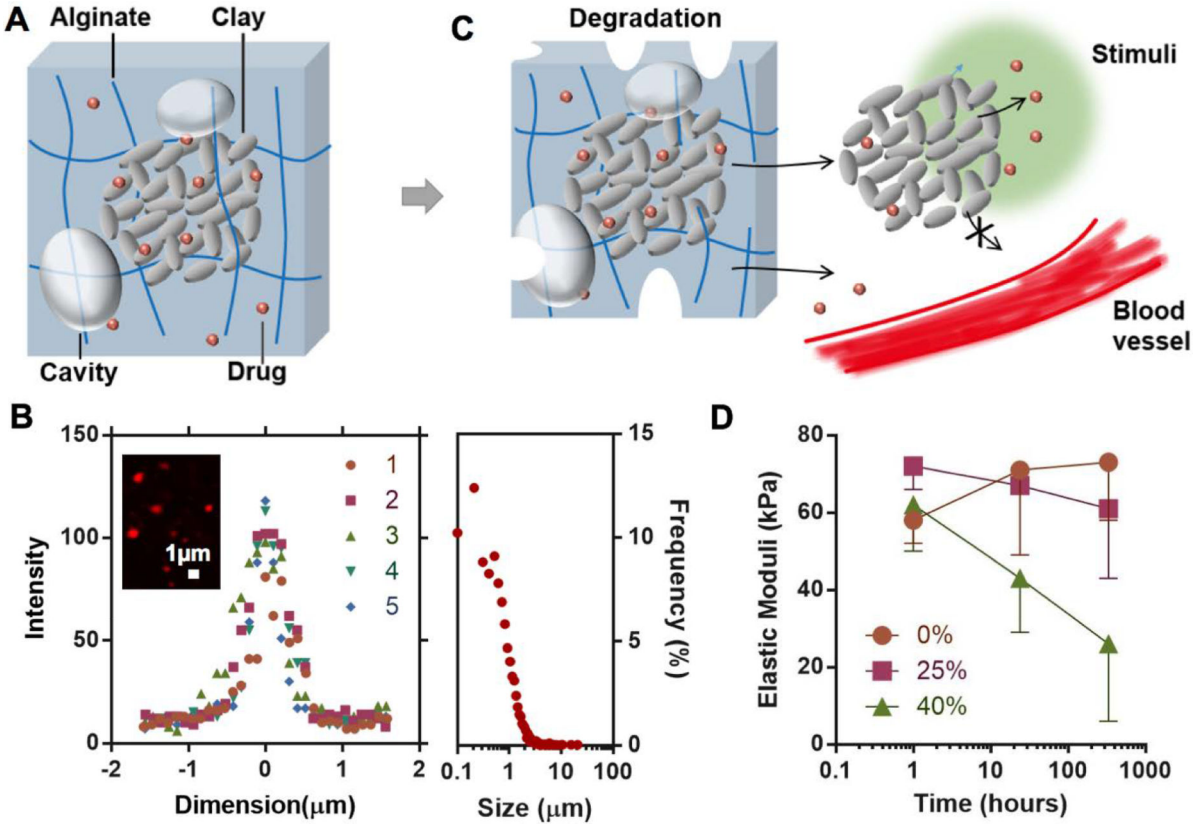

Figure 1.

Design of composite hydrogels for controlled drug delivery. A) Clay microparticles formed by nanoparticles of Laponite (grey discs) adsorb drug molecules (red) and reside inside a biodegradable alginate network (blue lines) with micro-sized cavities (grey bubbles). The hydrogels also encapsulate some free drugs that are not associated with the clay. B) Representative intensity-dimension profiles of individual particles (Left; N=5 batches) and the population size distribution of the clay microparticles inside the composite hydrogels (Right; counted particles N=3882). The inset shows a confocal image of the clay nanoparticles and microparticles highlighted with Rhodamine-B. C) The alginate network degrades slowly over time, accompanied with the release of the clay microparticles, clay nanoparticles and free drug. Subject to localized stimuli like the change in pH (green region), the clay particles are expected to release most of the loaded drug locally without systemic exposure. D) Elastic moduli, as a metric for degradation of the composite hydrogels, as a function of time and the fraction of oxidized alginate in the hydrogels. Data represents the mean ±SD; N=3 per group.

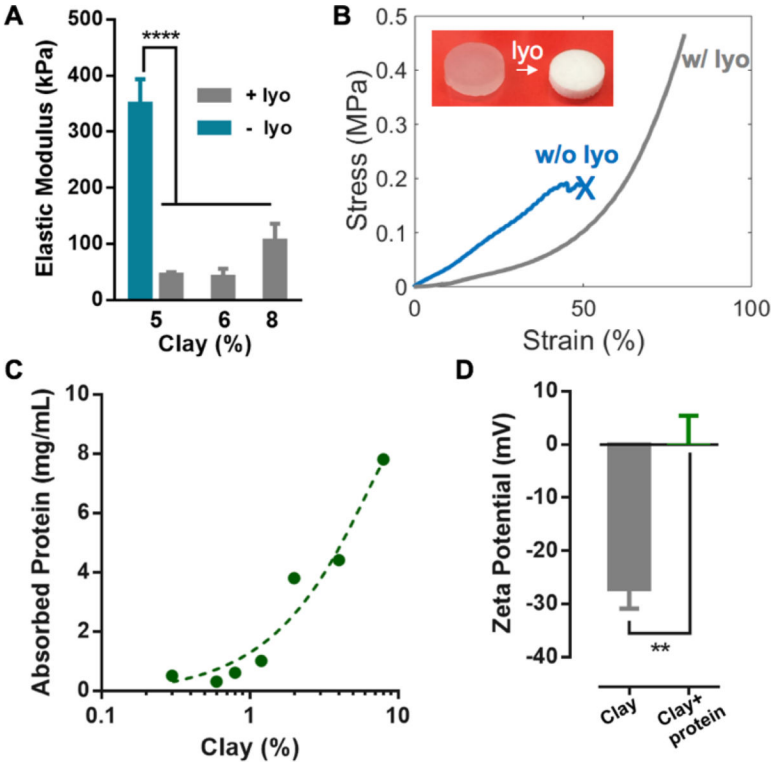

Figure 2.

Drug-loading and mechanical properties of the composite hydrogels. A) Elastic moduli of the composite hydrogels with different clay contents; the as-prepared hydrogels of 5% clay before lyophilization (blue bar) is included for comparison. Data represents the mean ±SD; N=3 per group. *P* values were determined by an ANOVA test; ****$P \leq 0.0001$. B) Compression stress-strain curves of the composite hydrogels (6% clay) before (w/o lyo) and after lyophilization (w/ lyo); the cross indicates gel rupture. The inset shows the composite hydrogels before and after lyophilization. C) Dependence of the IGF1 mimetic protein loading capacity on the clay content. The initial concentration of the protein was fixed at 8 mg/mL. D) Zeta potentials of the clay nanoparticles with and without adsorbed IGF1 mimetic protein. Data represents the mean ±SD; N=3 per group. *P* values were determined by a student t test; **$P \leq 0.01$.

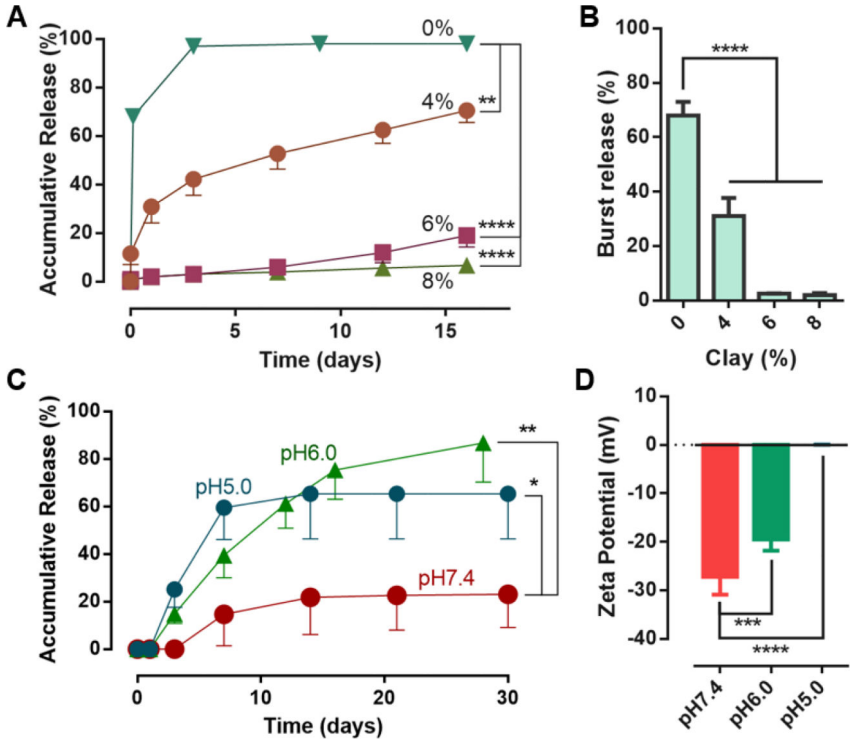

Figure 3.

In vitro drug-releasing properties. A) In vitro release profiles from the composite hydrogels with varying clay contents in cPBS medium of pH 7.4. B) Quantification of burst release measured by release within first 24 hours. C) Release profiles of composite hydrogels with 6% clay in release medium of varying pH. The ANOVA test was performed on the total amount of released drug. D) Zeta potentials of the clay nanoparticles at different pH. Data represents the mean ±SD; N=3 per group. *P* values were determined by ANOVA test; **P*≤0.05; ***P*≤0.01; ****P*≤0.001; *****P*≤0.0001.

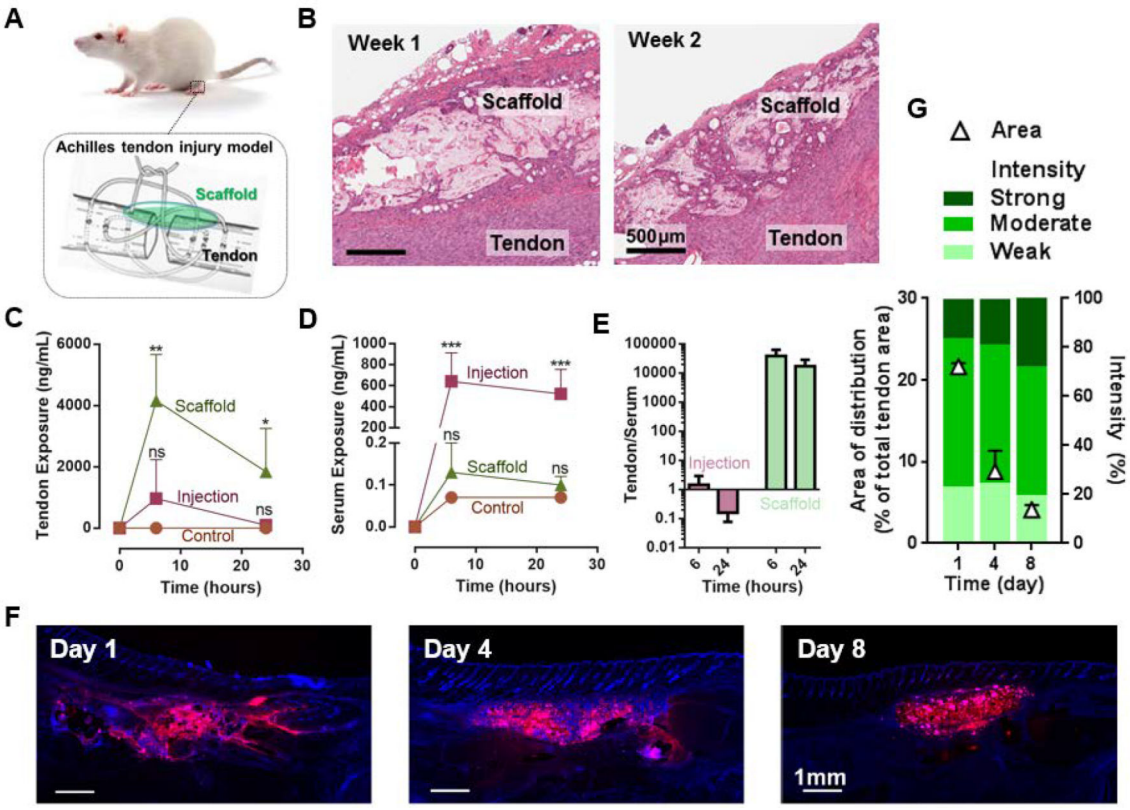

Figure 4.

In vivo extended and localized drug release. A) The rat model of Achilles tenotomy and treatment with drug-releasing scaffolds (green). B) Images of H&E stained histological sections of scaffolds of the composite hydrogel 1 week and 2 weeks after implantation on top of the site of Achilles tendon injury. C,D) IGF1 mimetic protein exposure to Achilles tendon (C) and to serum (D) as a function of time. Bolus injection of the same protein quantity (Injection), and injection of saline (Control) are included for comparison. Data represents the mean ±SD; N=4 per group. *P* values were determined by ANOVA tests; **P*≤0.05; ***P*≤0.01; ****P*≤0.001; ns, not significant. E) Ratio of the protein exposure in Achilles tendon to serum resulting from bolus injection and composite hydrogels at 6 and 24 hours. F) Fluorescent images of histological sections from explanted tissues with DAPI staining (blue) to examine the distribution of the fluorescein-labeled protein (red) in vivo over time. G) Area of distribution of the IGF1 mimetic protein (triangles) and fluorescence signal intensity over time of the IGF1 positive area (graded as Strong, Moderate, Weak protein signal). Data represents the mean ±SD; N=2 per group.

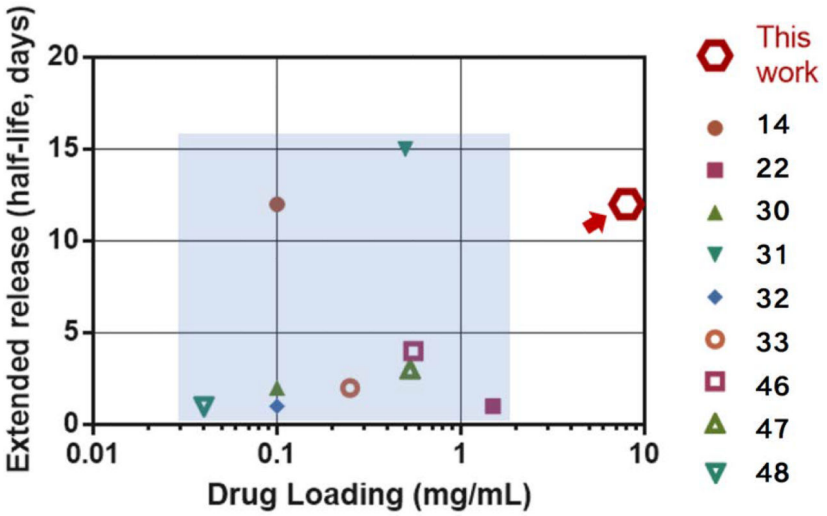

Figure 5.

Comparison of drug loading capacity and extended releasing properties of the composite hydrogels and other hydrogel delivery systems. The extended release is quantified by the time at which 50% of the loaded drug is released. The composite hydrogels (marked with red arrow) outperform existing hydrogel delivery systems (light blue area) in terms of drug loading and extended releasing properties. The reference number for each data point is as labeled (14,22,30–33,46–48).